Chem

Catalytic atroposelective macrocyclization for constructing dominant rotors in peptides

Graphical abstract

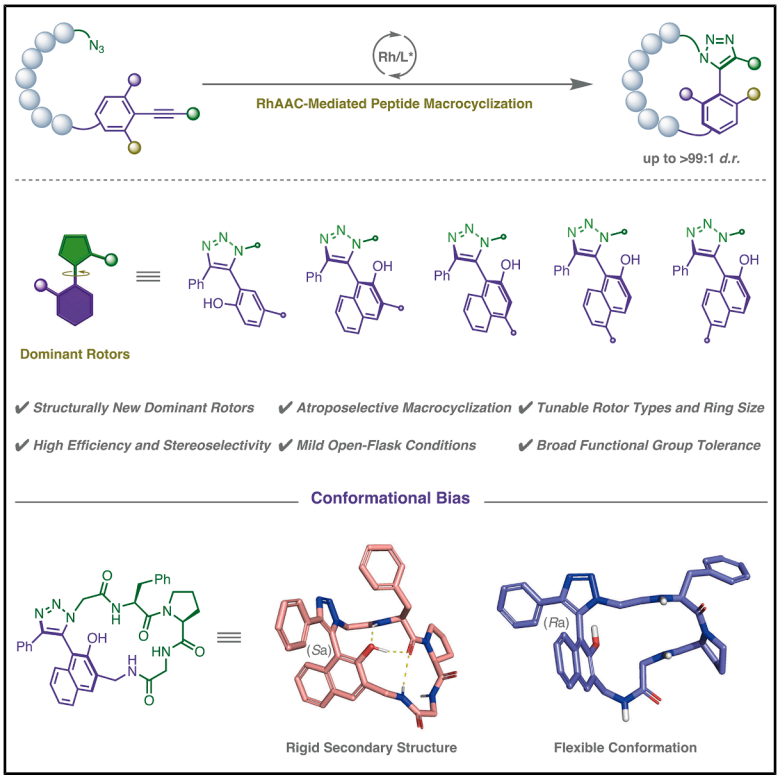

Highlights

- Structurally tunable triazole-based biaryls serve as dominant rotors in macrocycles
- Atroposelective peptide macrocyclization enables construction of dominant rotors
- Rotor configuration directs macrocycle organization and encodes conformational bias
- Efficient stereoselective access to structurally diverse axially chiral macrocycles

Authors

Linwei Zeng, Yang (Daniel) Ou, Tianyi Yang, ..., Andrew D. Bond, Andrei K. Yudin, David R. Spring

Correspondence

ayudin@chem.utoronto.ca (A.K.Y.), spring@ch.cam.ac.uk (D.R.S.)

In brief

A catalytic atroposelective macrocyclization strategy is developed to construct structurally tunable triazole-based dominant rotors in macrocyclic peptides. Different rotor configurations direct distinct macrocycle organizations and intramolecular interactions, leading to well-defined conformational states. This strategy enables atroposelective control in peptide macrocyclization and highlights the potential of axially chiral rotors as versatile structural elements for shaping macrocyclic architectures.

Zeng et al., 2026, Chem *12*, 103257
December 10, 2026
Published by Elsevier Inc.
https://doi.org/10.1016/j.chempr.2026.103257

CellPress

Please cite this article in press as: Zeng et al., Catalytic atroposelective macrocyclization for constructing dominant rotors in peptides, Chem (2026), https://doi.org/10.1016/j.chempr.2026.103257

Chem

CellPress
OPEN ACCESS

Article

Catalytic atroposelective macrocyclization for constructing dominant rotors in peptides

Linwei Zeng,[1] Yang (Daniel) Ou,[2,3] Tianyi Yang,[1,3] Alexander Rowley,[1] Peter Rukovanský,[1] Andrew D. Bond,[1] Andrei K. Yudin,[2,*] and David R. Spring[1,4,*]

[1]Yusuf Hamied Department of Chemistry, University of Cambridge, Lensfield Road, Cambridge CB2 1EW, UK
[2]Davenport Research Laboratories, Department of Chemistry, University of Toronto, 80 St. George Street, Toronto, ON M5S 3H6, Canada
[3]These authors contributed equally
[4]Lead contact
*Correspondence: ayudin@chem.utoronto.ca (A.K.Y.), spring@ch.cam.ac.uk (D.R.S.)
https://doi.org/10.1016/j.chempr.2026.103257

THE BIGGER PICTURE Controlling the conformational landscapes of macrocyclic peptides is central to understanding and optimizing their biological properties, yet predicting and manipulating these landscapes remains challenging because multiple structural elements can contribute to conformational preferences. The dominant rotor concept provides a structural approach to biasing the conformational landscapes of macrocycles toward two isolable atropisomeric states, but expanding this concept to unexplored structural motifs and developing methods for their stereoselective installation remain important challenges.

Our work develops a class of structurally tunable triazole-based dominant rotors and establishes an atroposelective macrocyclization strategy that directly constructs these configurationally stable, axially chiral biaryls within macrocyclic peptides. This macrocyclization enables atroposelective access to structurally diverse macrocycles while introducing a dominant rotor that can influence their conformational preferences. Importantly, the configurational state of the dominant rotor can direct the overall spatial arrangement of the macrocycle, leading to distinct patterns of intramolecular interactions, including hydrogen bonding, and thereby stabilizing different conformational states. This interplay offers an opportunity to access distinct and well-defined secondary structures of macrocyclic peptides. By combining atroposelective peptide macrocyclization with the dominant rotor concept, this work expands the structural and synthetic scope of dominant rotors and offers a strategy for encoding conformational bias into macrocyclic peptides. More broadly, it highlights the potential of stereochemically defined structural elements to shape the spatial organization and conformational landscapes of complex macrocycles.

SUMMARY

Three-dimensional conformations determine the physicochemical and biological properties of macrocycles. Axially chiral biaryl fragments, which are widely found in macrocyclic natural products and drugs, have been evaluated as dominant rotors in synthetic cyclic peptides. While the corresponding constructs are powerful tools for influencing backbone conformations of macrocycles, their stereoselective installation remains challenging and underexplored. Here, we report a catalytic atroposelective macrocyclization strategy for constructing dominant rotors from azido peptides incorporating aryl alkyne building blocks via intramolecular rhodium-catalyzed azide-alkyne cycloaddition (RhAAC). This macrocyclization delivers structurally diverse, ring-size-tunable macrocyclic peptides bearing triazole-based biaryl rotors with high atroposelectivity. Comprehensive NMR analyses, X-ray crystallography, and computational studies reveal key conformational features of macrocyclic products and elucidate the role of dominant rotors in dictating overall molecular conformation. This AAC-mediated atroposelective macrocyclization provides a versatile platform for accessing axially chiral macrocyclic peptides and expands the dominant rotor strategy toward stereochemically programmed conformational control.

Please cite this article in press as: Zeng et al., Catalytic atroposelective macrocyclization for constructing dominant rotors in peptides, Chem (2026), https://doi.org/10.1016/j.chempr.2026.103257

INTRODUCTION

Macrocyclic peptides and their mimetics have emerged as versatile and increasingly prominent scaffolds in modern drug discovery.[1–3] By virtue of their relatively large molecular size, extended surface area, and conformational preorganization, macrocyclic peptides may uniquely target protein-protein interactions (PPIs) and shallow allosteric binding sites on protein surfaces.[4,5] The physicochemical properties, proteolytic stability, and biological activities of peptide macrocycles are critically governed by their defined three-dimensional conformations, which dictate functional group orientation, interaction patterns, and cellular accessibility.[6] Over the years, a diverse array of strategies for peptide macrocyclization have been developed.[7–11] In particular, constrained motifs have been widely incorporated into macrocyclic peptides to rigidify and fine-tune backbone architectures, aiming to promote the mimicry of canonical secondary structures in proteins.[12–15] For example, structurally varied olefins, alkynes, heterocycles, highly strained cyclophanes, and bicyclo[2.2.1]pentanes (BCPs) have been introduced into macrocyclic peptides through a range of synthetic methodologies, including ring-closing metathesis (RCM), metal-catalyzed coupling, C–H functionalization, azide-alkyne cycloaddition (AAC), electrocatalysis, and enzyme catalysis.[16–26] Despite being effective, many existing strategies suffer from limitations, such as relatively low efficiency, limited structural diversity, and incomplete control over backbone conformational preference. Therefore, the development of structural units that enable precise and programmable conformational control in macrocyclic peptides remains highly desirable.

Atropisomers are prevalent in naturally occurring macrocyclic peptides, exemplified by vancomycin, the TMC-95 family, tryptorubin A, and cihunamide B, which possess wide-ranging biological activities (Figure 1A).[27–30] The corresponding atropisomeric motifs serve as key structural elements that confer the well-defined and intricate three-dimensional architecture of the molecular backbone, thereby contributing to the stabilization of biologically relevant conformations for molecular recognition and target binding. Moreover, installation of an atropisomeric biaryl unit can kinetically trap high-energy conformations of macrocycles that are typically thermodynamically disfavored, providing valuable insights into the spatial structural features of macrocyclic compounds.[31,32] In 2021, we introduced the concept of "dominant rotors" within macrocyclic systems.[33] In this framework, incorporation of a biaryl unit with a rotational barrier (>25 kcal · mol^{-1}) substantially exceeding those of other backbone torsions reorganizes the conformational energy landscape, leading to two isolable atropisomeric states with distinct macrocyclic conformation ensembles. This strategy was implemented using racemic triazole-containing biaryl amino acids installed into macrocyclic peptides via solid-phase peptide synthesis (SPPS) and amide-coupling macrocyclization, affording both atropisomeric products after separation (Figure 1B).[33,34] Beyond constraining conformational freedom, the axially chiral rotor biases peptide backbone conformations within the otherwise identical sequence, leading to atropisomer-dependent geometries that exhibit distinct intramolecular noncovalent interaction patterns and secondary structures. For instance, an (*S*)-configurational axially chiral rotor has been introduced to induce a single 3_{10}-helix secondary structure within a 22-membered macrocyclic peptide (Figure 1C).[35] The Miller group recently reported that an amide-based (*P*)-atropisomer within a macrocyclic peptide promoted the formation of an intriguing double β-turn, further highlighting the role of axial chirality in modulating peptide conformations.[36] We have pursued distinct types of dominant rotors and aimed to develop general atroposelective macrocyclization strategies for their chemodivergent installation, thereby facilitating access to macrocyclic peptides bearing biaryl rotors with defined stereochemistry. Achieving precise stereoselective and enantioselective control during macrocyclization has long been a formidable challenge.[37–40] Although a wide range of synthetic and biocatalytic strategies have enabled the assembly of axially chiral scaffolds[41–50] and medium-ring-bridged biaryl atropisomers,[51–57] the extension of atroposelective control to macrocyclization[57–59]—particularly within chemically diverse and conformationally complex peptide frameworks—remains largely unexplored (Figure 1D).[60–63] Addressing this challenge requires overcoming several key obstacles: (1) the pronounced conformational heterogeneity of peptides, together with competing transannular interaction networks, may generate energetically accessible reactive conformations and thereby limit stereochemical discrimination; (2) the substantial entropic penalties inherent to macrocyclization call for fast and efficient bond-forming reactions to achieve productive cyclization prior to conformational equilibration; and (3) achieving precise site-selective and atroposelective control in peptides bearing multiple amide bonds and Lewis base residues remains difficult due to potential catalyst perturbation and competing coordination events.

We have previously conducted a systematic investigation into AAC-enabled macrocyclization and peptide stapling, demonstrating the excellent compatibility of this type of chemistry with peptides.[22,64–67] In recent years, atroposelective AAC between *ortho*-substituted aryl alkynes and azides has been established as a powerful chemical tool for the synthesis of triazole-based atropisomers, offering high efficiency, excellent chemoselectivity and stereoselectivity, broad functional-group tolerance, as well as mild reaction conditions.[68–74] We envisaged that this emergent atroposelective AAC chemistry could be harnessed for peptide macrocyclization to embed biaryl frameworks, thereby expanding the structural diversity of dominant rotors and refining their stereoselective assembly into macrocycles. Herein, we validate this hypothesis and report the catalytic atroposelective installation of dominant rotors into macrocyclic peptides via AAC-type chemistry (Figure 1E). Through the incorporation of various alkynyl building blocks at different sites into azido-peptides, followed by rhodium-catalyzed AAC (RhAAC), atroposelective macrocyclization was achieved through four distinct linkage topologies: side (side-chain residue) azide-to-tail (C-terminal) alkyne, side azide-to-side alkyne, head (N-terminal) azide-to-tail alkyne, and side azide-to-head alkyne. These AAC-mediated macrocyclizations are operationally simple and highly tolerant of variations in peptide chain length and composition, enabling the efficient synthesis of structurally diverse, ring-size-tunable, conformationally constrained macrocyclic peptides bearing phenylene-triazole-based biaryl rotors. Remarkably, this method allows for the

Please cite this article in press as: Zeng et al., Catalytic atroposelective macrocyclization for constructing dominant rotors in peptides, Chem (2026), https://doi.org/10.1016/j.chempr.2026.103257

CellPress
OPEN ACCESS

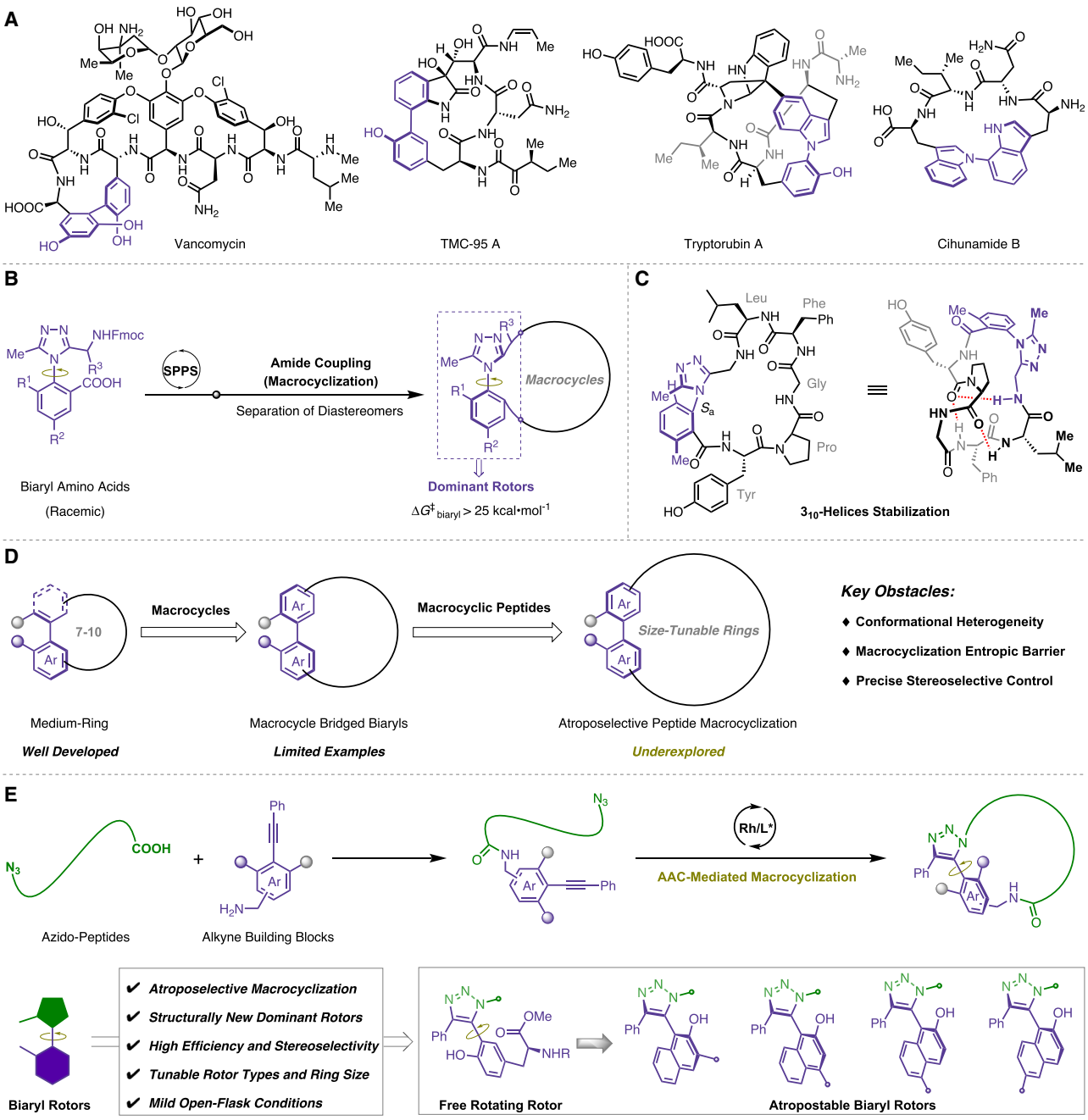

Figure 1. Dominant rotors in macrocycles

(A) Biaryl atropisomers in naturally occurring macrocycles with biological activities.

(B) Concept of dominant rotors: atropostable biaryl motifs with high rotational barriers (>25 kcal · mol^{-1}) partition the conformational landscape of macrocyclic peptides into two distinct, stable atropisomeric states.

(C) Induction and stabilization of 3_{10}-helix structures in macrocyclic peptides using the dominant rotor strategy.

(D) Atroposelective construction of ring-bridged biaryl frameworks.

(E) This work: AAC-mediated peptide macrocyclization for atroposelective construction of tunable dominant rotors.

selective incorporation of axially chiral rotors with defined stereochemistry into the macrocycle with high efficiency and atroposelectivity, overcoming the long-standing challenge of controlling chemoselectivity and enantioselectivity in peptide macrocyclization chemistry. Moreover, experimental and computational structural studies of the products elucidate the key role of designed dominant rotors in governing the conformations of macrocyclic peptides. This atroposelective macrocyclization provides a versatile platform for the synthesis of axially chiral macrocyclic peptides and broadens the scope of

Please cite this article in press as: Zeng et al., Catalytic atroposelective macrocyclization for constructing dominant rotors in peptides, Chem (2026), https://doi.org/10.1016/j.chempr.2026.103257

the dominant rotor strategy toward stereochemically programmed conformational control of peptide macrocycles.

RESULTS

Development of atroposelective macrocyclization

Initially, we introduced a phenylethynyl into tyrosine (Tyr) at the *ortho*-position of hydroxy and synthesized a dipeptide derivative **1a** to test the macrocyclization. The AAC reaction proceeded well in dichloromethane (DCM, 10 mM) at room temperature (RT) using $[Rh(cod)(OH)]_2$ (1 mol %) as the catalyst, affording the 14-membered macrocycle **2a** in 75% isolated yield (Figure 2A). However, the resulting triazole-based biaryl exhibited atropisomeric interconversion on the NMR timescale (class I atropisomer),[75] indicating that the rotational barrier was insufficient to confer configurationally stable axial chirality due to the small size of the *ortho*-hydrogen atom. This conclusion was further supported by density functional theory (DFT) calculations, which revealed a rotational barrier of 15.8 kcal · mol^{-1} ($t_{1/2,\ 25°C}$ = 43 ms) (for details, see supplemental information). To increase steric hindrance while simplifying the structure of the alkynyl building block, 3-(aminomethyl)-1-(phenylethynyl)naphthalen-2-ol (^{3}APN) was designed and prepared to further test our hypothesis (Figure 2B). In this design, the hydroxy group was retained to potentially induce atroposelectivity in the intramolecular cycloaddition and to serve as a hydrogen-bond donor and acceptor, which is expected to promote additional intramolecular hydrogen bonding and thus stabilize the overall molecular conformation. The optimization of the atroposelective macrocyclization of precursor **1b** is summarized in Figure 2C (Table S1). A preliminary reaction in DCM (5 mM) catalyzed by $[Rh(cod)(OH)]_2$ (1 mol %) gave a pair of 13-membered cyclic products in a good 70:30 diastereomeric ratio (dr), likely induced by the chiral nature of precursor **1b** (entry 1). The structure and configuration of the major diastereomer (*Sa*)-**2b** were confirmed by X-ray crystallography (Figure S3; Table S2). The combination of $[Rh(cod)(OH)]_2$ and the (*S*)-Carreira phosphoramidite ligand in DCM (10 mM) improved the dr to 97:3 and isolated (*Sa*)-**2b** in 89% yield (entry 2). Diluting the reaction to 5 mM increased the isolated yield to 94% while maintaining the same dr value (entry 3). A solvent screen revealed that this macrocyclization also proceeded efficiently in MeCN, EtOH, MeOH, dimethyl sulfoxide (DMSO), and an MeCN/PBS buffer mixture, providing excellent dr values and high isolated yields of (*Sa*)-**2b** (entries 4–8). Additionally, the use of the (*R*)-ligand reversed the atroposelectivity, affording a 45:55 dr and yielding (*Ra*)-**2b** and (*Sa*)-**2b** in 51% and 39% yield, respectively (entry 9). Subsequently, thermal interconversion experiments between (*Sa*)-**2b** and (*Ra*)-**2b** were conducted at 100°C in DMSO. The rotational barriers for the conversion from (*Sa*)-**2b** to (*Ra*)-**2b**, and vice versa, were determined to be 30.8 and 31.4 kcal · mol^{-1}, respectively, well exceeding the 25 kcal · mol^{-1} threshold that defines a dominant rotor[33] (Figures 2D and S1). Pleasingly, the two diastereomers of **2b** exhibited distinct retention times in high-performance liquid chromatography (HPLC) (Figure 2E) and distinguishable signals in NMR spectra (Figure 2F), demonstrating the high atropostability of this biaryl motif at RT. These results collectively show that biaryl motifs of this type can effectively serve as dominant rotors with high configurational stability in macrocyclic peptides.

Exploration of scope

Having established the AAC-mediated atroposelective macrocyclization, a substrate of AcNH-K(N_3)-A-CO-^{3}APN (**1c**) was then prepared (Figure 3A). Reactions with the (*S*)-ligand and (*R*)-ligand in DCM (0.5 mM) proceeded cleanly (Figure 3B), affording 91:9 and 11:89 dr and yielding (*Sa*)-**2c** and (*Ra*)-**2c** in 77% and 78% isolated yields, respectively. Having confirmed the structure of (*Ra*)-**2c** by X-ray crystallography (Figure S4; Table S2), we performed a thermal epimerization experiment from (*Sa*)-**2c** to (*Ra*)-**2c** in DMSO at 120°C, revealing a high rotational barrier of 33.2 kcal · mol^{-1} and a Gibbs free energy difference of +1.2 kcal · mol^{-1} (Figure 3C). NMR analyses and molecular dynamics (MD) simulations revealed that (*Sa*)-**2c** and (*Ra*)-**2c** adopt distinct solution conformations in DMSO-d_6 (Figure 3D), consistent with atropisomer-dependent modulation of the accessible conformational space. These differences were accompanied by distinct intramolecular hydrogen-bonding patterns, which arise within the conformational space defined by the dominant rotor. Specifically, no persistent hydrogen bonding is observed in (*Sa*)-**2c**, whereas (*Ra*)-**2c** exhibits an exocyclic interaction involving the alanine NH group. Notably, Ramachandran analysis indicated that the alanine residue occupies a β strand region in (*Ra*)-**2c** but shifts to a right-handed helical region in (*Sa*)-**2c**, highlighting atropisomer-dependent backbone conformational preferences (for details, see supplemental information). Importantly, the solution structure of (*Ra*)-**2c** closely matched its X-ray crystal structure, further supporting the consistency of the NMR and Ramachandran analyses. We then sought to enrich the structural diversity of dominant rotors by shifting the branched aminomethyl group of ^{3}APN to the 4-, 5-, and 6-positions of the naphthalene ring, furnishing linear precursors **1d**–**1f** to test the macrocyclization (Figure 3E). For **1d** and **1e**, the macrocyclizations efficiently resulted in products (*Sa*)-**2d** and (*Sa*)-**2e** in excellent yields with 98:2 dr values, among which the structure of (*Sa*)-**2e** was confirmed by X-ray crystallography (Figure S5; Table S2). With respect to **1f**, the macrocyclization proceeded in very low conversion, yielding (*Sa*)-**2f** in 8% yield with 89:11 dr. The thermal studies highlighted the remarkable atropostability of these biaryl rotors, with rotational barriers exceeding 35 kcal · mol^{-1} (Figure S2), demonstrating their potential as dominant rotors in macrocyclic peptides. By integrating these biaryl motifs with varied naphthylene-based cyclophane fragments, this atroposelective peptide macrocyclization demonstrates the ability to install dominant rotors with rich structural diversity and adjustable rigidity. Moreover, a precursor of 5-carboxy-1-(phenylethynyl)naphthalen-2-ol (^{5}CPN) was also prepared and incorporated into an azido-tripeptide sequence by SPPS to give **1a′**, which was selectively macrocyclized between side-chain azide and head alkyne using (*S*)- and (*R*)-ligands to deliver (*Sa*)-**2a′** and (*Ra*)-**2a′** with excellent dr values (Figure 3F). Although the SPPS strategy allows straightforward synthesis of this AAC precursor (**1a′**), the moderate yields and multiple solution conformations observed for both products ((*Sa*)-**2a′** and (*Ra*)-**2a′**) reflect the limitations of this specific cyclization mode.

Please cite this article in press as: Zeng et al., Catalytic atroposelective macrocyclization for constructing dominant rotors in peptides, Chem (2026), https://doi.org/10.1016/j.chempr.2026.103257

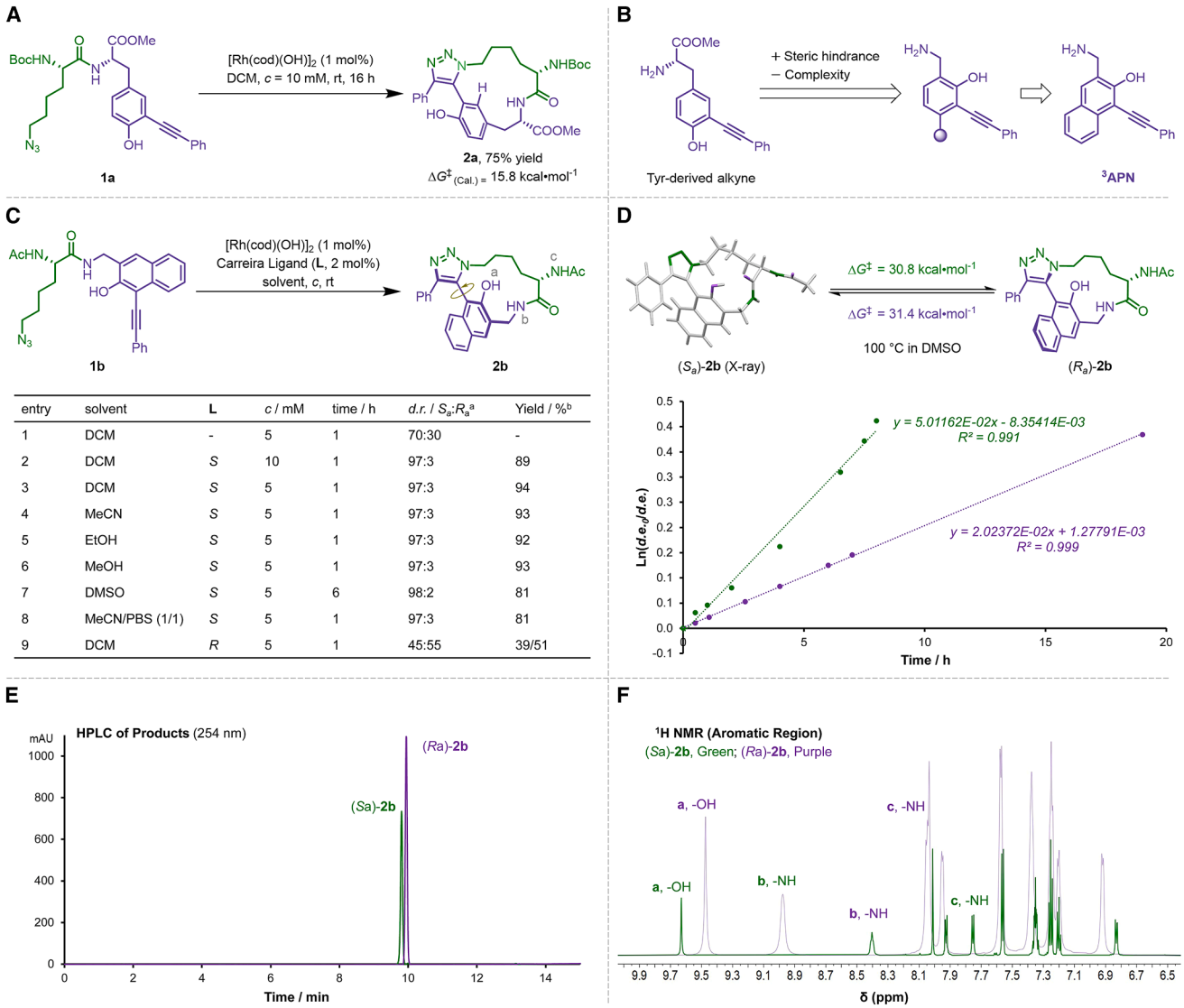

entry	solvent	L	c / mM	time / h	d.r. / S_a:R_a[a]	Yield / %[b]
1	DCM	-	5	1	70:30	-
2	DCM	*S*	10	1	97:3	89
3	DCM	*S*	5	1	97:3	94
4	MeCN	*S*	5	1	97:3	93
5	EtOH	*S*	5	1	97:3	92
6	MeOH	*S*	5	1	97:3	93
7	DMSO	*S*	5	6	98:2	81
8	MeCN/PBS (1/1)	*S*	5	1	97:3	81
9	DCM	*R*	5	1	45:55	39/51

Figure 2. Development of AAC-mediated atroposelective macrocyclization

(A) Preliminary macrocyclization of precursor **1a** afforded macrocycle **2a** as a pair of atropisomers that interconvert on the NMR timescale. DFT calculations indicated that the rotational barrier (15.8 kcal · mol^{-1}) was insufficient to stabilize the atropisomeric states.

(B) ^{3}APN was designed from the Tyr-derived alkyne by increasing steric hindrance while reducing chiral complexity.

(C) The development and optimization of the AAC-mediated atroposelective macrocyclization of precursor **1b** are summarized. [a]dr values refer to the ratio of (*Sa*)-**2b** to (*Ra*)-**2b**, as determined by HPLC; [b]yields refer to isolated products by silica gel column chromatography.

(D) Thermal interconversion in DMSO at 100°C revealed that the rotational barriers for (*Sa*)-**2b** ⇌ (*Ra*)-**2b** exceeded 30 kcal · mol^{-1}, sufficient to render the biaryl unit a dominant rotor in macrocycles.

(E) The HPLC traces (λ = 254 nm) of atropisomers (*Sa*)-**2b** and (*Ra*)-**2b** exhibit distinct retention times at RT.

(F) The ^{1}H NMR spectra of (*Sa*)-**2b** and (*Ra*)-**2b** exhibit sharp and distinct signals at RT.

We next evaluated the amino acid tolerance of our atroposelective macrocyclization by using ^{3}APN building blocks. The macrocyclization between side-chain azide and terminal alkyne was studied (Figure 4, top). An *N*-Boc-4-azido-2-aminobutyric acid (Boc-azido-DABA) derivative coupled with ^{3}APN was subjected to the macrocyclization under standard conditions (0.5 mM), affording the corresponding 11-membered macrocycle (*Sa*)-**2g** in 99:1 dr and 42% isolated yield, together with a dimeric byproduct in 20% yield (**2g**-dimer). For an ornithine-derived substrate, macrocyclization proceeded smoothly to generate the 12-membered macrocycle (*Sa*)-**2h** in 99:1 dr and 91% isolated yield. Numerous ε-azido lysine-derived linear materials with various protecting groups, including Boc and Cbz, were suitable for this atroposelective macrocyclization, leading to the corresponding 13-membered products in high yields with excellent atroposelectivity ((Sa)-**2i** to **2k**, 88%–95%, >96:4 dr). The extended linear peptides bearing diverse amino acids such as proline, alanine, phenylalanine, glycine, tryptophan, isoleucine,

Please cite this article in press as: Zeng et al., Catalytic atroposelective macrocyclization for constructing dominant rotors in peptides, Chem (2026), https://doi.org/10.1016/j.chempr.2026.103257

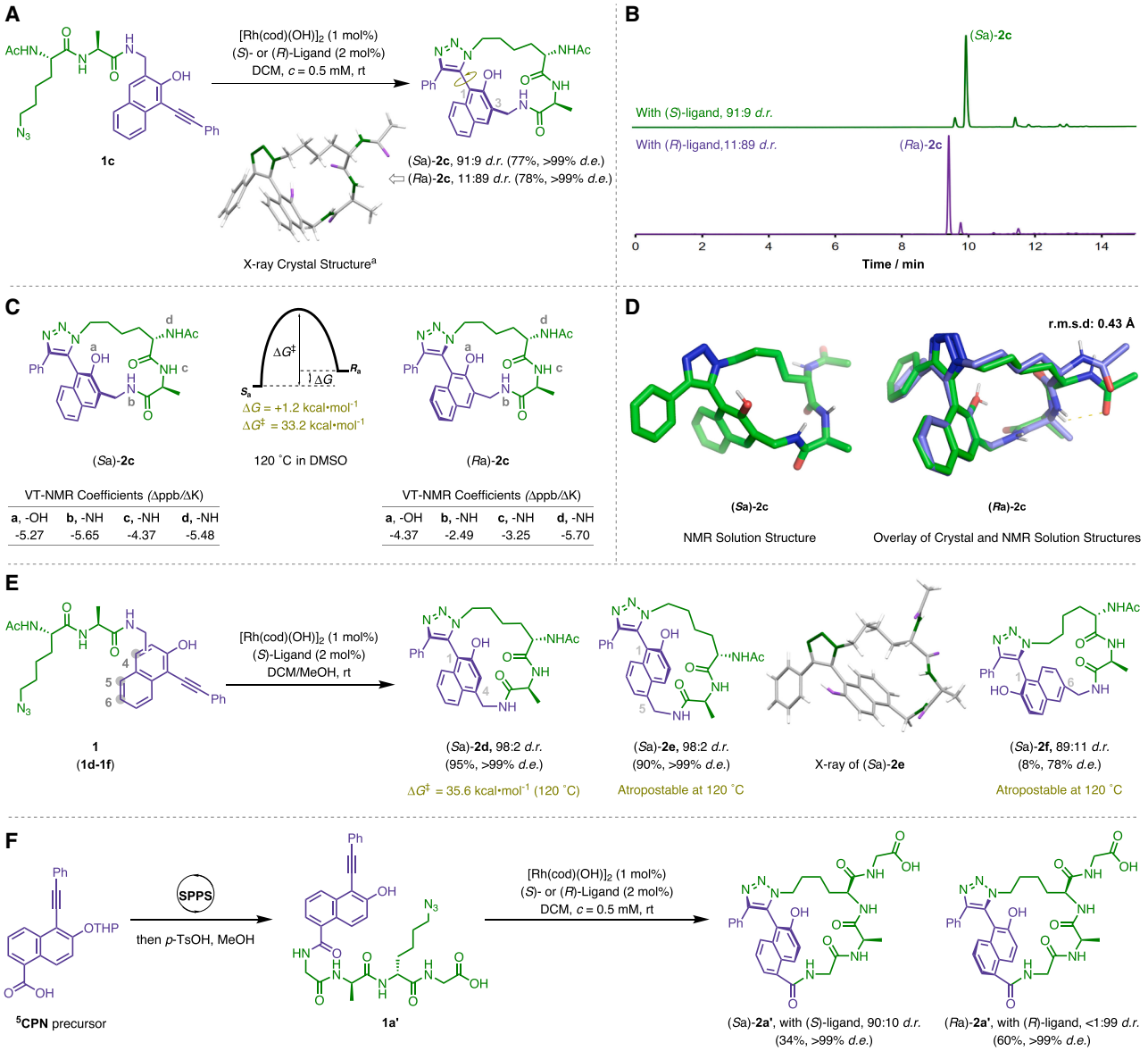

Figure 3. Exploration of structurally diverse rotors in macrocycles

(A) Atroposelective macrocyclization of precursor **1c** afforded (*Sa*)-**2c** and (*Ra*)-**2c** selectively using the corresponding Carreira ligand. [a]One molecule from the 2-fold twin crystal is shown.

(B) HPLC traces (λ = 254 nm) of the macrocyclization reactions of **1c** with the (*S*)-ligand and (*R*)-ligand indicate controllable atroposelectivity, leading to 91:9 and 11:89 dr for (*Sa*)- and (*Ra*)-**2c**, respectively.

(C) Thermal interconversion in DMSO at 120°C revealed that the rotational barrier for the interconversion of (*Sa*)-**2c** to (*Ra*)-**2c** was 33.2 kcal · mol^{-1}.

(D) NMR solution structures of (*Sa*)-**2c** and (*Ra*)-**2c** in DMSO-d_6 demonstrated distinct backbone architectures for the two atropisomers. The X-ray crystal structure (lavender) of (*Ra*)-**2c** showed good overlap with the NMR solution structure (green).

(E) A series of APN building blocks was used for the installation of structurally diverse rotors with rotational barriers of >35 kcal · mol^{-1}.

(F) Use of a ^{5}CPN unit in SPPS enables streamlined synthesis of precursor **1a**′ followed by the atroposelective macrocyclization to (*Sa*)-**2a**′ and (*Ra*)-**2a**′. Each macrocycle exhibits two NMR conformations in DMSO-d_6.

and methionine were all amenable to this AAC-based macrocyclization, atroposelectively delivering 16- to 25-membered macrocyclic products in decent yields with high dr values ((*Sa*)-**2l** to **2p**, 52%–92%, 96:4 to >99:1 dr). Ligand-free macrocyclization of a hexapeptide-derived substrate (CbzNH-K(N_3)-F-V-S(O*t*-Bu)-P-A-CO-^{3}APN) efficiently generated a pair of inseparable 28-membered products in 70% isolated yield (**2q**). However, the atroposelective variant using the (*S*)-Carreira ligand proceeded with very low conversion, likely due to the large steric hindrance of the ligand shutting down macrocyclization.

Subsequently, the macrocyclization between the side-chain azide and side-chain alkyne was explored (Figure 4, bottom). A

Please cite this article in press as: Zeng et al., Catalytic atroposelective macrocyclization for constructing dominant rotors in peptides, Chem (2026), https://doi.org/10.1016/j.chempr.2026.103257

CellPress
OPEN ACCESS

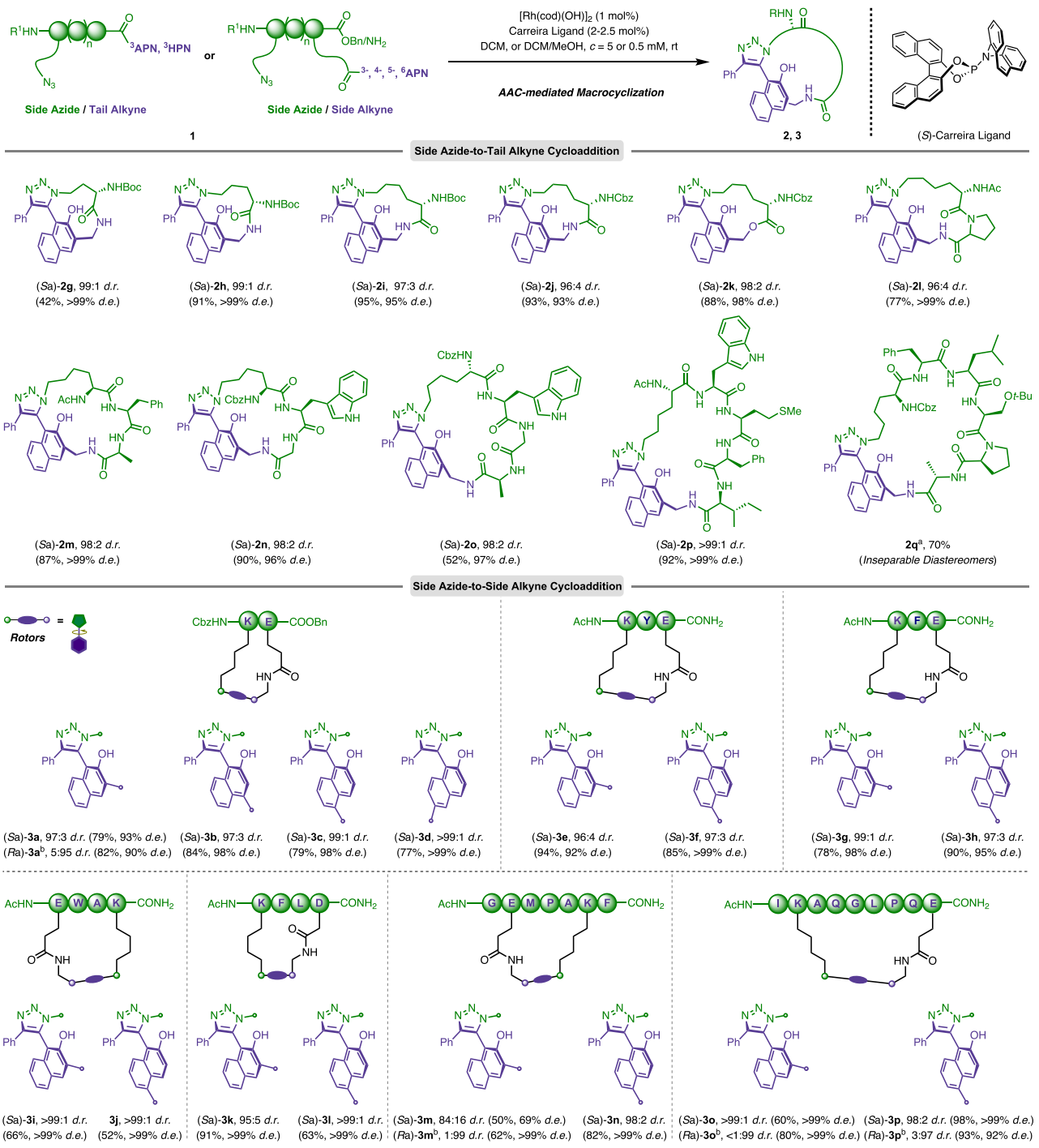

Figure 4. Substrate scope of macrocycles from side azide-to-tail alkyne and side azide-to-side alkyne cycloaddition

A mixture of linear starting materials, $[Rh(cod)(OH)]_2$ (1 mol %), and (*S*)-Carreira ligand (2 mol %) was dissolved in the indicated solvent (DCM or 1:1 DCM/MeOH, *c* = 5 or 0.5 mM) and stirred at RT. The reaction mixture was analyzed using HPLC to determine the dr values ((*Sa*):(*Ra*)). Yields and diastereomeric excess (de) in parentheses refer to isolated products. [a]Without ligand. [b]·(*R*)-Carreira ligand was used. [c]The dr value was determined by ^{1}H NMR analysis of the isolated product.

series of CbzNH-K(N_3)-E-COOBn derivatives functionalized by four APN building blocks were highly compatible with this atroposelective macrocyclization, yielding the corresponding macrocycles with (*S*)-configurational biaryls ((*Sa*)-**3a** to **3d**) with excellent dr (97:3 to >99:1) and decent isolated yields (77%–84%). Conversely, compound (*Ra*)-**3a** was efficiently afforded upon the use of the (*R*)-Carreira ligand, demonstrating late-stage divergence during the synthesis of macrocyclic peptides with

Please cite this article in press as: Zeng et al., Catalytic atroposelective macrocyclization for constructing dominant rotors in peptides, Chem (2026), https://doi.org/10.1016/j.chempr.2026.103257

Table 1. Macrocycles (12–18 membered rings) from head azide-to-tail alkyne cycloaddition

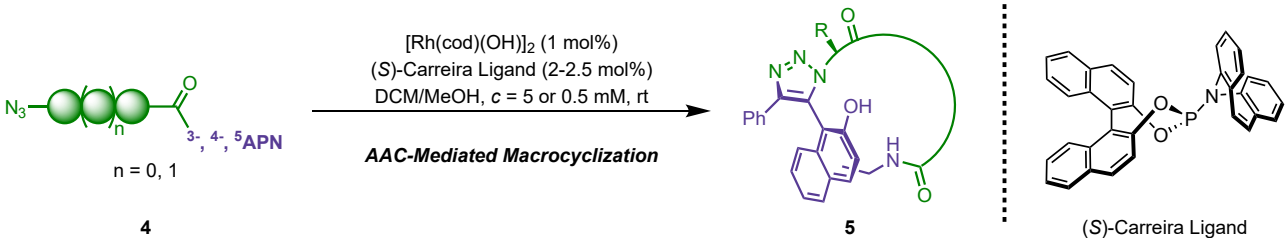

Precursors	Products	Ring size	dr of reactions[a]	Isolated yield (de[b])
N_3-G-Y-CO-^{3}**APN**	(*Sa*)-**5a**	12	98:2	81% (96%)
N_3-G-W-CO-^{3}**APN**	(*Sa*)-**5b**	12	94:6	88% (89%)
N_3-G-S-CO-^{3}**APN**	(*Sa*)-**5c**	12	97:3	65% (95%)
N_3-G-E-CO-^{3}**APN**	(*Sa*)-**5d**	12	99:1	81% (96%)
N_3-G-C(STrt)-CO-^{3}**APN**	(*Sa*)-**5e**	12	94:6	66% (86%)
N_3-G-K(NHBoc)-CO-^{3}**APN**	(*Sa*)-**5f**	12	93:7	76% (>99%)
N_3-G-H(NTrt)-CO-^{3}**APN**	(*Sa*)-**5g**	12	98:2	44% (>99%)
N_3-A-Y-CO-^{3}**APN**	(*Sa*)-**5h**	12	>99:1	77% (>99%)
N_3-G-W-G-CO-^{3}**APN**	(*Sa*)-**5i**	15	98:2	59% (96%)
N_3-G-W-G-CO-^{4}**APN**	(*Sa*)-**5j**	16	>99:1	78% (>99%)
N_3-G-W-G-CO-^{5}**APN**	(*Sa*)-**5k**	18	>99:1	66% (>99%)
N_3-V-W-G-CO-^{3}**APN**	**5l**[c]	15	>99:1	22% (>99%)
N_3-A-F-G-CO-^{3}**APN**	(*Sa*)-**5m**	15	93:7	93% (>99%)

Reaction conditions: a mixture of linear precursors, $[Rh(cod)(OH)]_2$, and (*S*)-ligand was dissolved in solvent (DCM or 1:1 DCM/MeOH, or 9:1 DCM/MeOH, *c* = 5 or 0.5 mM) and stirred at RT.

[a]The dr values were determined by HPLC analysis of reaction mixture.

[b]The de in parentheses refer to isolated products.

[c]The reaction was conducted in the absence of Carreira ligand.

defined axially chiral linkages. A series of sequences of tripeptides and tetrapeptides bearing diverse amino acids—including lysine, Tyr, phenylalanine, tryptophan, alanine, leucine, glutamic acid and aspartic acid—were evaluated for side-to-side macrocyclization with ^{3}APN and ^{5}APN, obtaining the corresponding macrocyclic products (**3e**–**3l**) with excellent dr (95:5 to >99:1) in satisfactory yields (52%–94%). Two longer unprotected peptide sequences with potentially helical structures, including AcNH-G-E-M-P-A-K(N_3)-F-$CONH_2$ and the caseicin A-derived antibacterial peptide AcNH-I-K(N_3)-A-Q-G-L-P-Q-E-$CONH_2$,[76] were coupled with ^{3}APN and ^{5}APN to explore the [i,i + 4] and [i,i + 7] stapling. The AAC-enabled atroposelective macrocyclization successfully afforded the (*Sa*)- and (*Ra*)-configured macrocyclic peptides (**3m**–**3p**) with high dr (84:16 to >99:1) and good isolated yields (50%–98%), depending on the ligand configuration. These results validated the application of our atroposelective macrocyclization in peptide stapling for the conformational rigidification and optimization of biologically relevant peptides.

We then turned our attention to the head-to-tail atroposelective macrocyclization mediated by AAC. A series of dipeptides and tripeptides containing structurally varied residues, including Tyr, tryptophan, serine, glutamine, cysteine, lysine, histidine, valine, alanine and glycine, were first examined (Table 1). Numerous dipeptides bearing a head glycine azide and a tail ^{3}APN unit underwent efficient macrocyclization to furnish the corresponding 12-membered products ((*Sa*)-**5a** to **5g**) in 44%–88% yields with excellent dr (93:7 to 99:1). Replacement of the glycine azide with a secondary alanine azide was also well tolerated, delivering the desired macrocycle (**5h**) in 77% yield and >99:1 dr. Subsequently, three linear precursors obtained by coupling N_3-G-W-G-COOH with ^{3}APN, ^{4}APN, and ^{5}APN units were subjected to atroposelective macrocyclization, successfully furnishing the corresponding 15-, 16-, and 18-membered macrocycles ((*Sa*)-**5i** to **5k**) in satisfactory yields (59%–78%) with outstanding stereoselectivity (>98:2 dr). Sequences bearing bulky head azido amino acids were also examined, each exclusively furnishing the pure diastereomer of the corresponding 15-membered macrocycle (**5l** or **5m**) in 22% and 93% yields, respectively. These results demonstrate the excellent tolerance of this atroposelective, AAC-mediated macrocyclization toward a wide range of functional groups and amino acid residues.

We next applied the ^{3}APN building block to explore longer peptide sequences in this atroposelective, head-to-tail AAC-based macrocyclization (Figure 5). An N_3-G-F-A-I-CO-^{3}APN sequence was treated under standard conditions using the (*S*)-ligand and (*R*)-ligand, giving the corresponding 15-membered (*Sa*)-**5n** and (*Ra*)-**5n** in the crude reaction mixture with dr values of 69:31 and 4:96, respectively. The N_3-G-F-P-G-CO-^{3}APN

Please cite this article in press as: Zeng et al., Catalytic atroposelective macrocyclization for constructing dominant rotors in peptides, Chem (2026), https://doi.org/10.1016/j.chempr.2026.103257

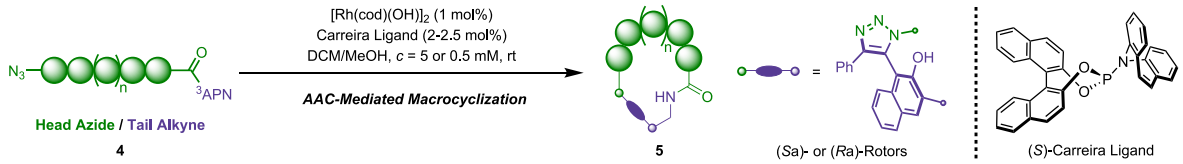

Head Azide-to-Tail Alkyne Cycloaddition

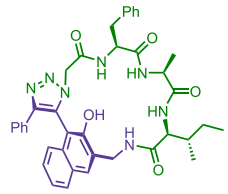

(*Sa*)-**5n**, 69:31 *d.r.* (67%, >99% *d.e.*)
(*Ra*)-**5n**[a], 4:96 *d.r.* (75%, >99% *d.e.*)

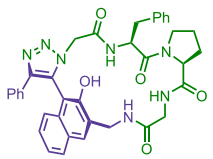

(*Sa*)-**5o**, 52:48 *d.r.* (33%, >99% *d.e.*)
(*Ra*)-**5o**[a], 4:96 *d.r.* (73%, >99% *d.e.*)

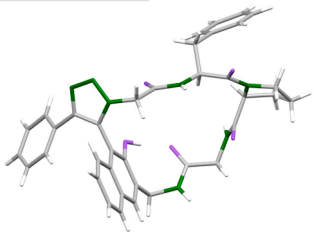

X-ray Crystal Structure of **(*Ra*)-5o**

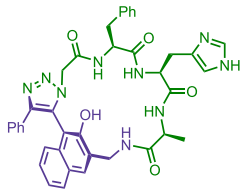

5p, N.R.

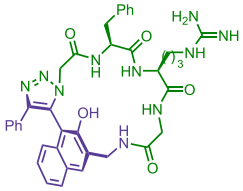

5q[b,c], 74:26 *d.r.*
(*Sa*)-**5q**, (30%, >99% *d.e.*)
(*Ra*)-**5q**, (8%, >99% *d.e.*)

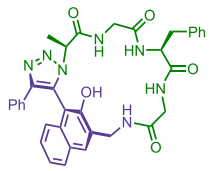

5r, >99:1 *d.r.* (80%, >99% *d.e.*)

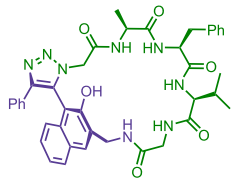

5s[b], 40:60 *d.r.*
(*Sa*)-**5s**, (31%, >99% *d.e.*)
(*Ra*)-**5s**, (58%, >99% *d.e.*)

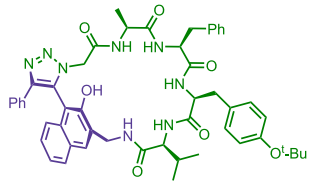

(*Sa*)-**5t**, 96:4 *d.r.* (58%, >99% *d.e.*)

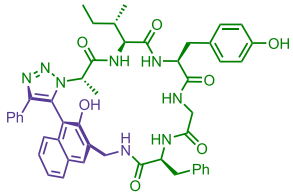

5u, >99:1 *d.r.* (59%,>99% *d.e.*)

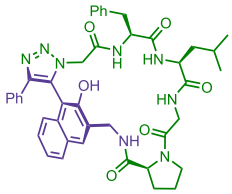

(*Sa*)-**5v**, 85:15 *d.r.* (40%, >99% *d.e.*)
(*Ra*)-**5v**[a], 2:98 *d.r.* (64%, >99% *d.e.*)

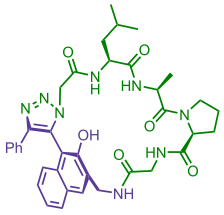

(*Sa*)-**5w**[d] (64%, >20:1 *d.r.*)
(*Ra*)-**5w**[a,d] (53%, 1:12 *d.r.*)

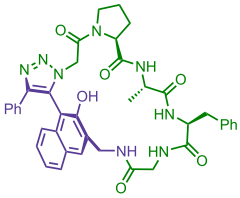

(*Sa*)-**5x**, 98:2 *d.r.* (78%, >99% *d.e.*)
(*Ra*)-**5x**, 4:96 *d.r.* (42%, >99% *d.e.*)

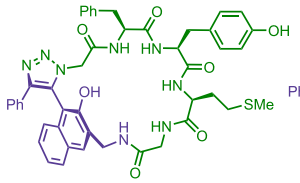

(*Sa*)-**5y**, 97:3 *d.r.* (43%, 93% *d.e.*)

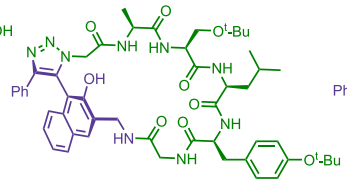

(*Sa*)-**5z**, 97:3 *d.r.* (73%, >99% *d.e.*)

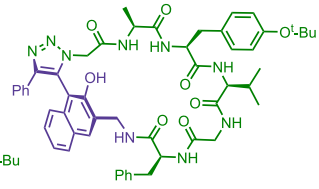

(*Sa*)-**5aa**, 59:41 *d.r.* (23%, 94% *d.e.*)
(*Ra*)-**5aa**[b], 37:63 *d.r.* (36%, 97% *d.e.*)

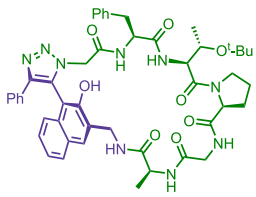

(*Sa*)-**5ab**, 63:37 *d.r.* (13%, >99% *d.e.*)
(*Ra*)-**5ab**[b], 16:84 *d.r.* (84%, >99% *d.e.*)

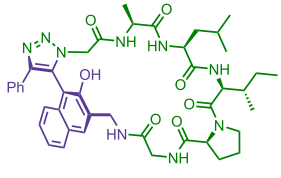

(*Sa*)-**5ac**, 95:5 *d.r.* (72%, >99% *d.e.*)
(*Ra*)-**5ac**[a], 3:97 *d.r.* (64%, >99% *d.e.*)

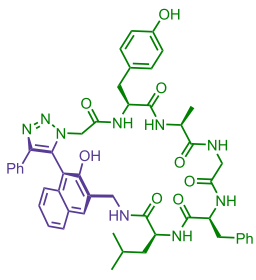

5ad[b], 42:58 *d.r.*
(*Sa*)-**5ad**, (24%,>99% *d.e.*)
(*Ra*)-**5ad**, (30%, >99% *d.e.*)

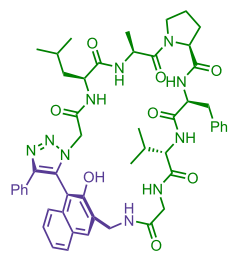

(*Sa*)-**5ae**, 90:10 *d.r.* (60%, >99% *d.e.*)
(*Ra*)-**5ae**[a], 4:96 *d.r.* (52%, >99% *d.e.*)

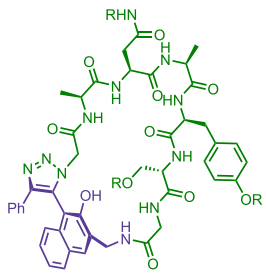

(*Sa*)-**5af**, R = PG[e], 86:14 *d.r.* (48%, 98% *d.e.*)
(*Sa*)-**5af**[c], R = H, 88:12 *d.r.* (34%, >99% *d.e.*)

(legend on next page)

Please cite this article in press as: Zeng et al., Catalytic atroposelective macrocyclization for constructing dominant rotors in peptides, Chem (2026), https://doi.org/10.1016/j.chempr.2026.103257

substrate was tested with the (*S*)-ligand and (*R*)-ligand as well, leading to a low 52:48 dr and an excellent 4:96 dr, respectively, because the chiral nature of the sequence favored the formation of the (*Ra*)-product. Each diastereomer of **5o** was successfully afforded, among which the structure and configuration of (*Ra*)-**5o** was verified by X-ray crystallography (Figure S6; Table S2). A linear precursor bearing an unprotected histidine failed to deliver the corresponding product **5p** under both standard and ligand-free conditions, likely owing to the strong coordinating ability of imidazole, which we hypothesize chelated and deactivated the rhodium catalyst. A sequence containing a Pbf-protected arginine was compatible with this chemistry to give a 74:26 dr after macrocyclization and deprotection, successfully isolating both atropisomers of the macrocycle ((*Sa*)-**5q** and (*Ra*)-**5q**). A precursor bearing an N-terminal alanine azide was subjected to this protocol to selectively afford the single configurational product (**5r**) in 80% isolated yield. When the linear structure of N_3-G-A-F-V-G-CO-^{3}APN was treated under the standard conditions, the reaction was almost suppressed in the presence of the (*S*)-ligand. In contrast, the ligand-free conditions proceeded to give a 40:60 dr, affording macrocycle **5s** as both atropisomers. Subsequently, an array of pentapeptide and hexapeptide precursors proved well tolerated, delivering the corresponding configurational-defined 18-membered (**5t**–**5y**, 85:15 to >99:1 dr) and 21-membered (**5z**–**5ac**, 59:41 to 97:3 dr) products in moderate to good yields with decent atroposelectivities. The macrocyclization of N_3-G-Y-A-G-F-L-CO-^{3}APN proceeded well under the ligand-free conditions with a 42:58 dr (**5ad**), and the two atropisomers were subsequently isolated in 24% and 30% yields. A heptapeptide precursor of N_3-G-L-A-P-F-V-G-CO-^{3}APN was well tolerated in this macrocyclization, selectively furnishing 90:10 and 4:96 dr values using the (*S*)-ligand and (*R*)-ligand and yielding the corresponding (*Sa*)-**5ae** and (*Ra*)-**5ae**, respectively. Finally, a fully protected heptapeptide substrate was tested in a one-pot atroposelective macrocyclization/deprotection sequence, which gave an 88:12 dr and enabled the isolation of the 27-membered (*Sa*)-**5af** in 34% yield. These findings highlight the broad tolerance of this macrocyclization toward diverse amino acid compositions and ring sizes in macrocyclic peptides, therefore establishing a robust platform for the atroposelective incorporation of structurally diverse axially chiral biaryl rotors into peptide macrocycles. To rationalize the observed atroposelectivity, we proposed a plausible mechanism for this macrocyclization based on our previous work (Figure S10).[73]

Structural and conformational analyses

To further validate the role of installed dominant rotors in governing the conformational behavior of macrocyclic peptides, we performed detailed structural and conformational analyses on head-to-tail macrocyclization products using comprehensive NMR spectroscopy in conjunction with MD simulations (Figure S7). We initially focused on the two atropisomers of macrocycle **5o**, which were designed to incorporate a Gly-Pro motif as a turn-inducing element to facilitate β-turn nucleation.[77,78] As anticipated, (*Sa*)-**5o** adopts a type IV β-turn between the Phe residue and the naphthyl (Nap) unit. Within this conformational space defined by the (*Sa*)-atropisomeric rotor, the endocyclic phenolic group functions as both a hydrogen-bond donor and acceptor, allowing for the formation of two intramolecular hydrogen bonds (IMHBs) (Figure 6A). Such dual hydrogen-bonding behavior is rare within the conformational landscape of cyclic peptides and is associated with substantial backbone rigidification.[79] Ramachandran plot analysis reveals that Phe and Pro populate dihedral angles proximal to the β sheet region, while Gly resides in the left-handed helical region. In contrast, the (*Ra*)-**5o** exhibits a markedly different solution structure, consistent with an alternative atropisomer-defined conformational ensemble (Figure 6B). In this case, neither variable-temperature (VT) NMR experiments nor MD simulations provided evidence for the existence of IMHBs. Correspondingly, Ramachandran analysis indicates that Pro adopts dihedral angles characteristic of right-handed helical regions, whereas Phe remains confined to the β sheet-favored conformational space.

Recent work from the Yudin group demonstrated that the incorporation of short peptide sequences into macrocycles containing sterically hindered biaryl rotors can stabilize a 3_{10}-helical conformation.[35] Building on this concept, we sought to investigate how variations in the substituent pattern of a dominant biaryl rotor modulate the conformational landscape of related macrocycles. To this end, a YPGFL-containing precursor (N_3-G-Y-P-G-F-L-CO-^{3}APN) was prepared and tested in this atroposelective macrocyclization (Figure 6C). In the presence of the (*S*)-ligand and (*R*)-ligand, the macrocyclization proceeded efficiently, giving (*Sa*)-**5ag** and (*Ra*)-**5ag** in 97:3 and 11:89 dr, respectively. The enantiopure (*Sa*)-**5ag** and (*Ra*)-**5ag** could then be readily obtained for investigation of their solution structures. Macrocycle (*Ra*)-**5ag** was observed by NMR to exist as two major conformers in solution in an approximate 3:1 ratio. In the dominant conformer ((*Ra*)-**5ag**-maj), the peptide backbone adopts an overall β sheet-like secondary structure, in which a pair of parallel IMHBs are observed (Figure 6D). A type II β-turn is observed between Phe and Tyr, while a π-turn is formed between Tyr and Leu. Ramachandran plot analysis indicates that Tyr and Pro occupy β sheet-favored regions within negative-ϕ space, whereas Leu and Gly populate positive-ψ regions. Notably, Phe resides in the lower-right quadrant of the Ramachandran plot, a region that is only rarely populated in protein structures.[80] By contrast, the minor conformer observed in DMSO-d_6 ((*Ra*)-**5ag**-min) exhibits two distinct IMHBs, consistent

Figure 5. Substrate scope of macrocycles from head azide-to-tail alkyne cycloaddition

A mixture of linear peptide, $[Rh(cod)(OH)]_2$ (1 mol %), and (*S*)-Carreira ligand (2 mol %) was dissolved in the indicated solvent (DCM, 1:1 DCM/MeOH, or 9:1 DCM/MeOH, *c* = 5, 1, or 0.5 mM) and stirred at RT. The reaction mixture was analyzed by HPLC to determine the dr ((*Sa*):(*Ra*)). Yields and de in parentheses refer to isolated products. [a](*R*)-Carreira ligand was used. [b]The reaction was conducted without ligand due to the low conversion of ligand-assisted macrocyclization. [c]The data were acquired from the macrocyclization of the protected precursor followed by deprotection. [d]The dr values were determined via ^{1}H NMR analysis of the isolated products because the diastereomers were inseparable using HPLC. [e]PG represents protecting groups, with *t*-Bu on the hydroxyl group and triphenylmethyl (Trt) on the amide nitrogen.

Please cite this article in press as: Zeng et al., Catalytic atroposelective macrocyclization for constructing dominant rotors in peptides, Chem (2026), https://doi.org/10.1016/j.chempr.2026.103257

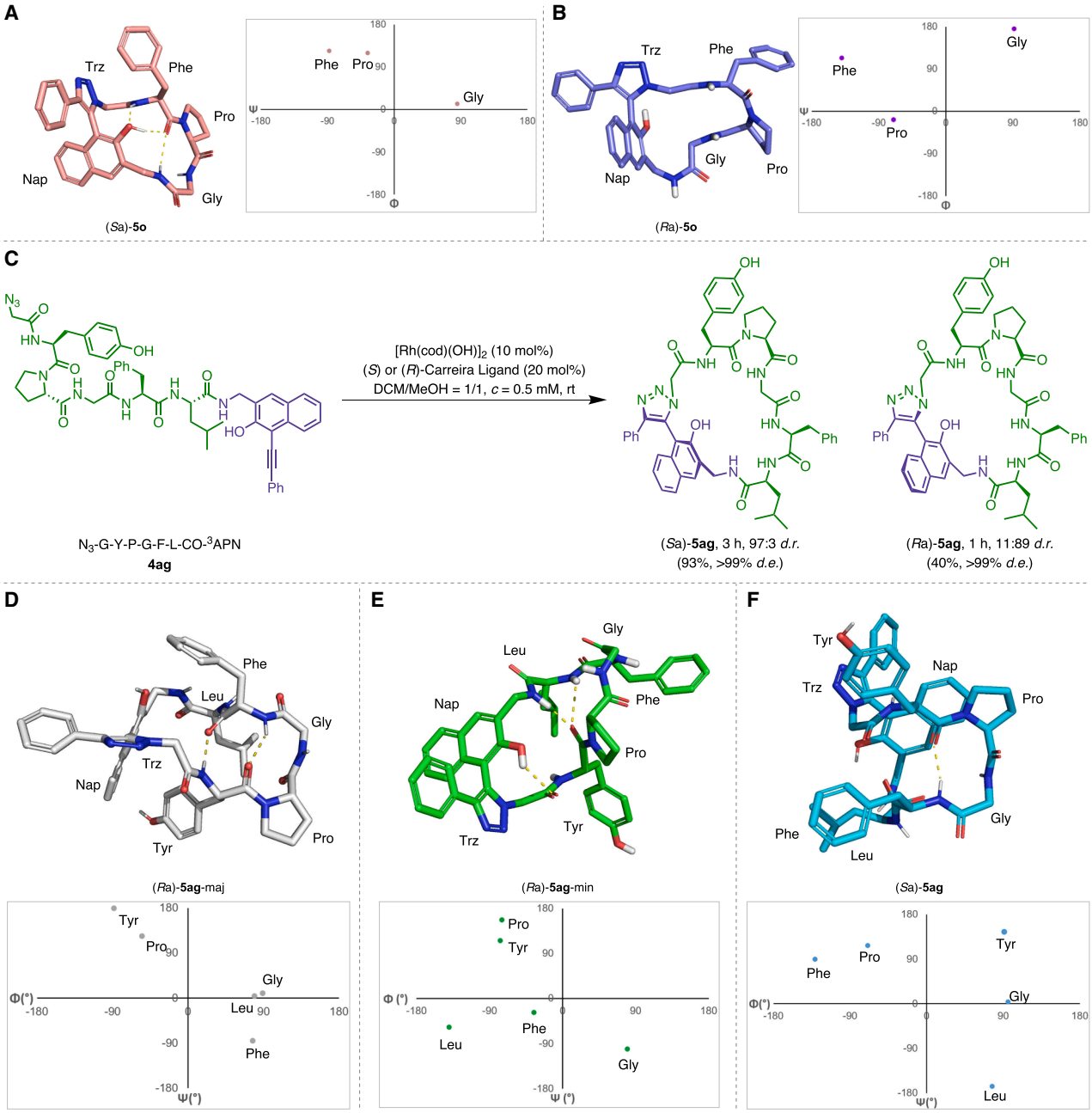

Figure 6. Structural analysis of selected macrocyclic peptides with naphthalene-triazole dominant rotors

(A) The endocyclic phenol group acts as both a hydrogen-bond donor and acceptor in the solution structure of (*Sa*)-**5o**, leading to a type IV β-turn between the Phe residue and the naphthyl (Nap) unit.

(B) The solution structure of (*Ra*)-**5o** was determined/generated from MD simulations, revealing a distinct conformation from that of (*Sa*)-**5o**.

(C) Atroposelective macrocyclization of a YPGFL-containing precursor (**4ag**) afforded (*Sa*)-**5ag** and (*Ra*)-**5ag** selectively.

(D) The major conformation ((*Ra*)-**5ag**-maj) of (*Ra*)-**5ag** in solution and its Ramachandran plot analysis.

(E) The minor conformation ((*Ra*)-**5ag**-min) of (*Ra*)-**5ag** in solution and its Ramachandran plot analysis.

(F) The solution structure of the (*Sa*)-**5ag** and its Ramachandran plot analysis.

with alternative backbone conformations involving α-turn and π-turn (Figure 6E). Unlike the major conformer, Leu and Phe in (*Ra*)-**5ag**-min adopt negative-ϕ dihedral angles characteristic of right-handed helical regions, while Tyr and Pro remain within the β sheet-associated conformational space. Interestingly, the endocyclic phenol, which shows the same features as in (*Sa*)-**5o**, forms an IMHB with the adjacent triazole amide's carbonyl. With respect to the atropisomer (*Sa*)-**5ag**, this macrocyclic

Please cite this article in press as: Zeng et al., Catalytic atroposelective macrocyclization for constructing dominant rotors in peptides, Chem (2026), https://doi.org/10.1016/j.chempr.2026.103257

peptide exhibits a distinct conformational profile. Careful inspection of the NMR spectra and HPLC-UV traces reveal a single dominant conformation in DMSO-d_6 with an approximate 10:1 population ratio. The major conformer displays a type II β-turn between Tyr and Phe, as supported by both NMR experiments and MD simulations (Figure 6F). Ramachandran plot analysis shows that Tyr occupies regions with positive ϕ/ψ values, while Leu is located in the lower-right quadrant of the plot—both of which are rarely populated for these amino acids in canonical protein structures.[80] Notably, the conformationally constrained nature of these macrocycles is accompanied by enhanced plasma stability. While the linear precursor **4ag** underwent extensive degradation and was nearly completely consumed within 120 h, both atropisomeric macrocycles, (*Sa*)-**5ag** and (*Ra*)-**5ag**, remained essentially unchanged over 7 days in human plasma (Figure S9; Table S4).

We further computed normalized principal moment ratios (NPR1 = I_1/I_3, NPR2 = I_2/I_3) for atropisomers and solution conformers of **5o** and **5ag** (Table S3), mapping them onto the standard principal moments of inertia (PMI) shape space bounded by rod-, disk-, and sphere-like reference geometries (Figure S8). This analysis reveals pronounced configuration-dependent segregation in global shape space, demonstrating that axial chirality of the dominant rotor governs the overall three-dimensional shape of the macrocyclic peptides.

DISCUSSION

We developed a catalytic atroposelective macrocyclization strategy to construct dominant rotors in peptides. This RhAAC-mediated macrocyclization methodology encompasses side azide-to-tail alkyne, side azide-to-side alkyne, side azide-to-head alkyne, and head azide-to-tail alkyne modes, delivering structurally diverse, ring-size controllable, and conformationally constrained macrocyclic peptides bearing triazole-linked biaryl rotors with high efficiency and excellent stereoselectivity. Comprehensive NMR analyses, X-ray crystallography, and computational studies of representative macrocyclic products elucidated the key conformational features of these macrocycles and highlighted the tunable role of installed dominant rotors in dictating the overall molecular conformation depending on its axial chirality. Overall, this stereoselective macrocyclization provides a versatile platform for the synthesis of axially chiral peptide macrocycles and expands the realm of stereochemically programmed conformational control mediated by dominant rotors, offering significant potential for peptide-based therapeutics with well-defined three-dimensional architectures.

METHODS

General procedures for the AAC-mediated atroposelective macrocyclization of peptides

The starting linear peptide (**1**, **4**, and **1′**) was dissolved in DCM or a mixture of DCM/MeOH (1:1 or 9:1) at the desired concentration at RT. Catalytic $[Rh(cod)(OH)]_2$ (1 mol %) and the (*S*)- or (*R*)-Carreira ligand (2 mol %) were then added at once. The reaction was further stirred at RT for the specified time, and progress was monitored via thin-layer chromatography (TLC) or HPLC. After completion, the reaction mixture was analyzed by HPLC to determine the dr value of products. The mixture was concentrated and purified by silica gel column chromatography, reverse-phase C18 column chromatography, or preparative HPLC to yield macrocyclic products (**2**, **3**, **5**, and **2′**). Further details regarding the methods can be found in the supplemental information.

RESOURCE AVAILABILITY

Lead contact

Further information and requests for resources should be directed to, and will be fulfilled by, the lead contact, David R. Spring (spring@ch.cam.ac.uk).

Materials availability

All materials generated in this study are available from the lead contact without restriction.

Data and code availability

The data supporting the findings of this study are available within the article and its supplemental information. Crystallographic data for the structures reported in this article have been deposited at the Cambridge Crystallographic Data Centre, under deposition numbers CCDC 2532764 (for (*Sa*)-**2b**), CCDC 2532762 (for (*Ra*)-**2c**), CCDC 2532763 (for (*Sa*)-**2e**), and CCDC 2532761 (for (*Ra*)-**5o**). Copies of the data are available free of charge at https://www.ccdc.cam.ac.uk/structures. All other data are available in the main text or the supplemental information.

ACKNOWLEDGMENTS

We gratefully acknowledge the Bill & Melinda Gates Foundation, AstraZeneca, UK Research and Innovation (UKRI), and the Natural Sciences and Engineering Research Council of Canada (NSERC) for financial support. The authors thank Dr. Peter Gierth (Department of Chemistry, University of Cambridge) for his assistance and valuable discussions regarding the NMR studies. L.Z. acknowledges Dr. Jin-Xiang Ye (Department of Chemistry, National University of Singapore) for support with the computational study of the rotational barrier of compound **2a** and Prof. Jianzhong Liu (School of Chemistry and Materials Science, University of Science and Technology of China) for helpful discussions and suggestions.

AUTHOR CONTRIBUTIONS

L.Z. conceived the idea, designed the experiments, and drafted the manuscript; L.Z., T.Y., A.R., and P.R. performed the synthetic experiments and analyzed the data; T.Y. conducted the stability studies; Y.D.O. designed and carried out the structural studies and PMI analysis under the supervision of A.K.Y.; A.D.B. performed the X-ray crystallographic analysis; D.R.S. supervised the research and provided overall guidance; all authors discussed the results and commented on the manuscript.

DECLARATION OF INTERESTS

The authors declare no competing interests.

SUPPLEMENTAL INFORMATION

Supplemental information can be found online at https://doi.org/10.1016/j.chempr.2026.103257.

Received: April 4, 2026
Revised: June 17, 2026
Accepted: August 20, 2026

REFERENCES

1. Colas, K., Bindl, D., and Suga, H. (2024). Selection of nucleotide-encoded mass libraries of macrocyclic peptides for inaccessible drug targets. Chem. Rev. *124*, 12213–12241. https://doi.org/10.1021/acs.chemrev.4c00422.
2. Swenson, C.S., Mandava, G., Thomas, D.M., and Moellering, R.E. (2024). Tackling undruggable targets with designer peptidomimetics and synthetic biologics. Chem. Rev. *124*, 13020–13093. https://doi.org/10.1021/acs.chemrev.4c00423.
3. Ji, X., Nielsen, A.L., and Heinis, C. (2024). Cyclic peptides for drug development. Angew. Chem. Int. Ed. *63*, e202308251. https://doi.org/10.1002/anie.202308251.
4. Buyanova, M., and Pei, D. (2022). Targeting intracellular protein-protein interactions with macrocyclic peptides. Trends Pharmacol. Sci. *43*, 234–248. https://doi.org/10.1016/j.tips.2021.11.008.
5. Vinogradov, A.A., Yin, Y., and Suga, H. (2019). Macrocyclic peptides as drug candidates: Recent progress and remaining challenges. J. Am. Chem. Soc. *141*, 4167–4181. https://doi.org/10.1021/jacs.8b13178.
6. White, C.J., and Yudin, A.K. (2011). Contemporary strategies for peptide macrocyclization. Nat. Chem. *3*, 509–524. https://doi.org/10.1038/nchem.1062.
7. Reguera, L., and Rivera, D.G. (2019). Multicomponent reaction toolbox for peptide macrocyclization and stapling. Chem. Rev. *119*, 9836–9860. https://doi.org/10.1021/acs.chemrev.8b00744.
8. Mortensen, K.T., Osberger, T.J., King, T.A., Sore, H.F., and Spring, D.R. (2019). Strategies for the diversity-oriented synthesis of macrocycles. Chem. Rev. *119*, 10288–10317. https://doi.org/10.1021/acs.chemrev.9b00084.
9. Sarojini, V., Cameron, A.J., Varnava, K.G., Denny, W.A., and Sanjayan, G. (2019). Cyclic tetrapeptides from nature and design: A review of synthetic methodologies, structure, and function. Chem. Rev. *119*, 10318–10359. https://doi.org/10.1021/acs.chemrev.8b00737.
10. Fang, P., Pang, W.-K., Xuan, S., Chan, W.-L., and Leung, K.C.-F. (2024). Recent advances in peptide macrocyclization strategies. Chem. Soc. Rev. *53*, 11725–11771. https://doi.org/10.1039/d3cs01066j.
11. He, J., Ghosh, P., and Nitsche, C. (2024). Biocompatible strategies for peptide macrocyclisation. Chem. Sci. *15*, 2300–2322. https://doi.org/10.1039/d3sc05738k.
12. Jwad, R., Weissberger, D., and Hunter, L. (2020). Strategies for fine-tuning the conformations of cyclic peptides. Chem. Rev. *120*, 9743–9789. https://doi.org/10.1021/acs.chemrev.0c00013.
13. Appavoo, S.D., Huh, S., Diaz, D.B., and Yudin, A.K. (2019). Conformational control of macrocycles by remote structural modification. Chem. Rev. *119*, 9724–9752. https://doi.org/10.1021/acs.chemrev.8b00742.
14. Hill, T.A., Shepherd, N.E., Diness, F., and Fairlie, D.P. (2014). Constraining cyclic peptides to mimic protein structure motifs. Angew. Chem. Int. Ed. *53*, 13020–13041. https://doi.org/10.1002/anie.201401058.
15. Smolyar, I.V., Yudin, A.K., and Nenajdenko, V.G. (2019). Heteroaryl rings in peptide macrocycles. Chem. Rev. *119*, 10032–10240. https://doi.org/10.1021/acs.chemrev.8b00789.
16. Frost, J.R., Scully, C.C.G., and Yudin, A.K. (2016). Oxadiazole grafts in peptide macrocycles. Nat. Chem. *8*, 1105–1111. https://doi.org/10.1038/nchem.2636.
17. Liu, X.-Y., Cai, W., Ronceray, N., Radenovic, A., Fierz, B., and Waser, J. (2023). Synthesis of fluorescent cyclic peptides via gold(I)-catalyzed macrocyclization. J. Am. Chem. Soc. *145*, 26525–26531. https://doi.org/10.1021/jacs.3c09261.
18. Osberger, T.J., Rogness, D.C., Kohrt, J.T., Stepan, A.F., and White, M.C. (2016). Oxidative diversification of amino acids and peptides by small-molecule iron catalysis. Nature *537*, 214–219. https://doi.org/10.1038/nature18941.
19. Yang, P., Širvinskas, M.J., Li, B., Heller, N.W., Rong, H., He, G., Yudin, A.K., and Chen, G. (2023). Teraryl braces in macrocycles: Synthesis and conformational landscape remodeling of peptides. J. Am. Chem. Soc. *145*, 13968–13978. https://doi.org/10.1021/jacs.3c03512.
20. Zhang, X., Lu, G., Sun, M., Mahankali, M., Ma, Y., Zhang, M., Hua, W., Hu, Y., Wang, Q., Chen, J., et al. (2018). A general strategy for synthesis of cyclophane-braced peptide macrocycles via palladium-catalysed intramolecular sp^3 C-H arylation. Nat. Chem. *10*, 540–548. https://doi.org/10.1038/s41557-018-0006-y.
21. Maruyama, H., Yamada, Y., Igarashi, Y., Matsuda, K., and Wakimoto, T. (2025). Enzymatic peptide macrocyclization via indole-N-acylation. Chem. Sci. *16*, 3872–3877. https://doi.org/10.1039/d4sc07839j.
22. Lau, Y.H., Wu, Y., Rossmann, M., Tan, B.X., de Andrade, P., Tan, Y.S., Verma, C., McKenzie, G.J., Venkitaraman, A.R., Hyvönen, M., et al. (2015). Double strain-promoted macrocyclization for the rapid selection of cell-active stapled peptides. Angew. Chem. Int. Ed. *54*, 15410–15413. https://doi.org/10.1002/anie.201508416.
23. Hu, X., Cao, Z., Chen, M., Huang, C.-D., Ni, S.-F., Zhang, S.-K., and Ruan, Z. (2025). Electrochemical late-stage stitching of tryptophan peptides via N–S bond formation. Angew. Chem. Int. Ed. *64*, e202517101. https://doi.org/10.1002/anie.202517101.
24. Biswas, K., Huang, C., Josien, H., Wan, M., Ding, F.-X., Zhu, Y., Sun, Z., Johnston, J.M., Palani, A., Lin, S., et al. (2024). Macrocyclic peptides targeting kras. WIPO Patent WO/2024/020159 A1.
25. Miller, S.J., Blackwell, H.E., and Grubbs, R.H. (1996). Application of ring-closing metathesis to the synthesis of rigidified amino acids and peptides. J. Am. Chem. Soc. *118*, 9606–9614. https://doi.org/10.1021/ja961626l.
26. Oueis, E., Jaspars, M., Westwood, N.J., and Naismith, J.H. (2016). Enzymatic macrocyclization of 1,2,3-triazole peptide mimetics. Angew. Chem. Int. Ed. *55*, 5842–5845. https://doi.org/10.1002/anie.201601564.
27. Lin, S., Yang, Z.Q., Kwok, B.H.B., Koldobskiy, M., Crews, C.M., and Danishefsky, S.J. (2004). Total synthesis of TMC-95A and -B via a new reaction leading to Z-enamides. Some preliminary findings as to SAR. J. Am. Chem. Soc. *126*, 6347–6355. https://doi.org/10.1021/ja049821k.
28. Okano, A., Isley, N.A., and Boger, D.L. (2017). Total syntheses of vancomycin-related glycopeptide antibiotics and key analogues. Chem. Rev. *117*, 11952–11993. https://doi.org/10.1021/acs.chemrev.6b00820.
29. Wyche, T.P., Ruzzini, A.C., Schwab, L., Currie, C.R., and Clardy, J. (2017). Tryptorubin A: A polycyclic peptide from a fungus-derived streptomycete. J. Am. Chem. Soc. *139*, 12899–12902. https://doi.org/10.1021/jacs.7b06176.
30. Yu, L., Nagata, Y., and Nakamura, H. (2024). Atroposelective total synthesis of cihunamide B. J. Am. Chem. Soc. *146*, 2549–2555. https://doi.org/10.1021/jacs.3c11016.
31. Diamandas, M., Heller, N.W., and Yudin, A.K. (2023). Nitrilium ion trapping as a strategy to access structurally diverse heterobiaryl-containing peptide macrocycles. Chem. Sci. *14*, 9482–9487. https://doi.org/10.1039/d3sc03058j.
32. Meyer, F.M., Collins, J.C., Borin, B., Bradow, J., Liras, S., Limberakis, C., Mathiowetz, A.M., Philippe, L., Price, D., Song, K., et al. (2012). Biaryl-bridged macrocyclic peptides: Conformational constraint via carbogenic fusion of natural amino acid side chains. J. Org. Chem. *77*, 3099–3114. https://doi.org/10.1021/jo202105v.
33. Diaz, D.B., Appavoo, S.D., Bogdanchikova, A.F., Lebedev, Y., McTiernan, T.J., Dos Passos Gomes, G., and Yudin, A.K. (2021). Illuminating the dark conformational space of macrocycles using dominant rotors. Nat. Chem. *13*, 218–225. https://doi.org/10.1038/s41557-020-00620-y.
34. McTiernan, T.J., Diaz, D.B., Saunders, G.J., Sprang, F., and Yudin, A.K. (2022). Navigating complex peptide structures using macrocycle conformational maps. RSC Chem. Biol. *3*, 739–747. https://doi.org/10.1039/d2cb00016d.
35. Širvinskas, M.J., Saunders, G.J., Mitrache, M., and Yudin, A.K. (2024). Stabilization of 3_{10}-helices in macrocycles using dominant rotor

methodology. J. Am. Chem. Soc. *146*, 24085–24093. https://doi.org/10.1021/jacs.4c08129.

36. Knudson, I.J., Dover, T.L., Dilworth, D.A., Paloutzian, C., Paz, O., Lin, J., Cho, H., Gonen, T., Schepartz, A., and Miller, S.J. (2026). Chemical and ribosomal synthesis of atropisomeric and macrocyclic peptides with embedded quinolines. Nat. Chem. *18*, 61–72. https://doi.org/10.1038/s41557-025-01935-4.
37. Rackl, J.W., Boll, L.B., and Wennemers, H. (2026). Organocatalyst-controlled stereoselective head-to-tail macrocyclizations. Science *391*, 931–936. https://doi.org/10.1126/science.aec8992.
38. Gagnon, C., Godin, É., Minozzi, C., Sosoe, J., Pochet, C., and Collins, S.K. (2020). Biocatalytic synthesis of planar chiral macrocycles. Science *367*, 917–921. https://doi.org/10.1126/science.aaz7381.
39. Guerrero-Morales, J., Scaglia, M., Fauran, E., Lepage, G., and Collins, S.K. (2024). Chemoenzymatic synthesis of macrocycles via dynamic kinetic resolution of secondary alcohols. Nat. Synth. *3*, 1275–1282. https://doi.org/10.1038/s44160-024-00591-9.
40. Lamartina, C.W., Chartier, C.A., Hirano, J.M., Shah, N.H., and Rovis, T. (2024). Crafting unnatural peptide macrocycles via Rh(III)-catalyzed carboamidation. J. Am. Chem. Soc. *146*, 20868–20877. https://doi.org/10.1021/jacs.4c05248.
41. Cheng, J.K., Xiang, S.-H., Li, S., Ye, L., and Tan, B. (2021). Recent advances in catalytic asymmetric construction of atropisomers. Chem. Rev. *121*, 4805–4902. https://doi.org/10.1021/acs.chemrev.0c01306.
42. Liu, C.-X., Zhang, W.-W., Yin, S.-Y., Gu, Q., and You, S.-L. (2021). Synthesis of atropisomers by transition-metal-catalyzed asymmetric C-H functionalization reactions. J. Am. Chem. Soc. *143*, 14025–14040. https://doi.org/10.1021/jacs.1c07635.
43. Schmidt, T.A., Hutskalova, V., and Sparr, C. (2024). Atroposelective catalysis. Nat. Rev. Chem. *8*, 497–517. https://doi.org/10.1038/s41570-024-00618-x.
44. Wencel-Delord, J., Panossian, A., Leroux, F.R., and Colobert, F. (2015). Recent advances and new concepts for the synthesis of axially stereoenriched biaryls. Chem. Soc. Rev. *44*, 3418–3430. https://doi.org/10.1039/c5cs00012b.
45. Xiang, S.-H., Ding, W.-Y., Wang, Y.-B., and Tan, B. (2024). Catalytic atroposelective synthesis. Nat. Catal. *7*, 483–498. https://doi.org/10.1038/s41929-024-01138-z.
46. Roos, C.B., Schulert, S.L., Zetzsche, L.E., McMinn, S.E., Cheong, A.E., Shim, E., Kwan, E.E., and Narayan, A.R.H. (2025). Synthesis of enantioenriched atropisomers by biocatalytic deracemization. Nature *647*, 648–655. https://doi.org/10.1038/s41586-025-09738-w.
47. Chen, Y.-B., Yang, Y.-N., Huo, X.-Z., Ye, L.-W., and Zhou, B. (2023). Recent advances in the construction of axially chiral arylpyrroles. Sci. China Chem. *66*, 2480–2491. https://doi.org/10.1007/s11426-023-1671-y.
48. Cao, R.-F., and Chen, Z.-M. (2023). Catalytic asymmetric synthesis of sulfur-containing atropisomers by C−S bond formations. Sci. China Chem. *66*, 3331–3346. https://doi.org/10.1007/s11426-023-1811-1.
49. Zhang, Z.-X., Zhai, T.-Y., and Ye, L.-W. (2021). Synthesis of axially chiral compounds through catalytic asymmetric reactions of alkynes. Chem Catal. *1*, 1378–1412. https://doi.org/10.1016/j.checat.2021.09.011.
50. Da, B.-C., Xiang, S.-H., Li, S., and Tan, B. (2021). Chiral phosphoric acid catalyzed asymmetric synthesis of axially chiral compounds. Chin. J. Chem. *39*, 1787–1796. https://doi.org/10.1002/cjoc.202000751.
51. Jia, S., Hao, Y., Li, Y., and Lan, Y. (2025). Chiral medium-sized rings beyond central chirality. Nat. Rev. Chem. *9*, 617–633. https://doi.org/10.1038/s41570-025-00735-1.
52. Newton, C.G., Braconi, E., Kuziola, J., Wodrich, M.D., and Cramer, N. (2018). Axially chiral dibenzazepinones by a palladium(0)-catalyzed atropo-enantioselective C-H arylation. Angew. Chem. Int. Ed. *57*, 11040–11044. https://doi.org/10.1002/anie.201806527.
53. Lu, S., Ong, J.-Y., Yang, H., Poh, S.B., Liew, X., Seow, C.S.D., Wong, M.W., and Zhao, Y. (2019). Diastereo- and atroposelective synthesis of bridged biaryls bearing an eight-membered lactone through an organocatalytic cascade. J. Am. Chem. Soc. *141*, 17062–17067. https://doi.org/10.1021/jacs.9b08510.
54. Du, J.-Y., Balan, T., Claridge, T.D.W., and Smith, M.D. (2022). Counterion-mediated enantioconvergent synthesis of axially chiral medium rings. J. Am. Chem. Soc. *144*, 14790–14797. https://doi.org/10.1021/jacs.2c05485.
55. Jia, S., Tian, Y., Li, X., Wang, P., Lan, Y., and Yan, H. (2022). Atroposelective construction of nine-membered carbonate-bridged biaryls. Angew. Chem. Int. Ed. *61*, e202206501. https://doi.org/10.1002/anie.202206501.
56. Liu, S.-J., Wang, X., Yang, J.-X., Ao, X.-S., Ni, S.-F., Zhang, Y.-C., and Shi, F. (2025). Atroposelective construction of axially chiral alkenylindole-fused nine-membered rings via catalytic asymmetric formal (4 + 5) cycloaddition. Nat. Commun. *16*, 6605. https://doi.org/10.1038/s41467-025-62035-y.
57. Qu, B.-L., Xiao, M., He, L., Shi, J.-W., Zhang, Z., Xiao, W.-J., and Lu, L.-Q. (2025). Enantioselective macrocyclization via catalytic metallic dipole relay. Nat. Catal. *8*, 368–377. https://doi.org/10.1038/s41929-025-01322-9.
58. Groh, M., Meidlinger, D., Bringmann, G., and Speicher, A. (2012). Atroposelective heck macrocyclization: Enantioselective synthesis of bis(bibenzylic) natural products. Org. Lett. *14*, 4548–4551. https://doi.org/10.1021/ol302132s.
59. Xi, J., and Gu, Z. (2020). Palladium-catalzyed atroposelective 16-membered macrocyclization: Total synthesis of isoplagiochin D. Chin. J. Chem. *38*, 1081–1085. https://doi.org/10.1002/cjoc.202000051.
60. Libman, A., Ben-Lulu, M., Gaster, E., Bera, R., Shames, A.I., Shaashua, O., Vershinin, V., Torubaev, Y., and Pappo, D. (2023). Multicopper clusters enable oxidative phenol macrocyclization (OxPM) of peptides. J. Am. Chem. Soc. *145*, 21002–21011. https://doi.org/10.1021/jacs.3c06978.
61. Padhi, C., Zhu, L., Chen, J.Y., Huang, C., Moreira, R., Challis, G.L., Cryle, M.J., and van der Donk, W.A. (2025). Biosynthesis of biphenomycin-like macrocyclic peptides by formation and cross-linking of ortho-tyrosines. J. Am. Chem. Soc. *147*, 23781–23796. https://doi.org/10.1021/jacs.5c06044.
62. Nguyen, D.T., Zhu, L., Gray, D.L., Woods, T.J., Padhi, C., Flatt, K.M., Mitchell, D.A., and van der Donk, W.A. (2024). Biosynthesis of macrocyclic peptides with C-terminal β-amino-α-keto acid groups by three different metalloenzymes. ACS Cent. Sci. *10*, 1022–1032. https://doi.org/10.1021/acscentsci.4c00088.
63. Ogawa, H., Nagata, Y., Chan, T.K., Matsuda, Y., and Nakamura, H. (2025). Rapid construction of a Tyr C6-Trp C5' linkage: Application in the total synthesis of micitide 982, a noncanonical cyclic peptide. Angew. Chem. Int. Ed. *64*, e202516053. https://doi.org/10.1002/anie.202516053.
64. Beckmann, H.S.G., Nie, F., Hagerman, C.E., Johansson, H., Tan, Y.S., Wilcke, D., and Spring, D.R. (2013). A strategy for the diversity-oriented synthesis of macrocyclic scaffolds using multidimensional coupling. Nat. Chem. *5*, 861–867. https://doi.org/10.1038/nchem.1729.
65. Nie, F., Kunciw, D.L., Wilcke, D., Stokes, J.E., Galloway, W.R.J.D., Bartlett, S., Sore, H.F., and Spring, D.R. (2016). A multidimensional diversity-oriented synthesis strategy for structurally diverse and complex macrocycles. Angew. Chem. Int. Ed. *55*, 11139–11143. https://doi.org/10.1002/anie.201605460.
66. Xu, W., Lau, Y.H., Fischer, G., Tan, Y.S., Chattopadhyay, A., de la Roche, M., Hyvönen, M., Verma, C., Spring, D.R., and Itzhaki, L.S. (2017). Macrocyclized extended peptides: Inhibiting the substrate-recognition domain of tankyrase. J. Am. Chem. Soc. *139*, 2245–2256. https://doi.org/10.1021/jacs.6b10234.
67. Isidro-Llobet, A., Murillo, T., Bello, P., Cilibrizzi, A., Hodgkinson, J.T., Galloway, W.R.J.D., Bender, A., Welch, M., and Spring, D.R. (2011). Diversity-oriented synthesis of macrocyclic peptidomimetics. Proc. Natl. Acad. Sci. USA *108*, 6793–6798. https://doi.org/10.1073/pnas.1015267108.
68. Zhang, X., Li, S., Yu, W., Xie, Y., Tung, C.H., and Xu, Z. (2022). Asymmetric azide-alkyne cycloaddition with Ir(I)/squaramide cooperative catalysis: Atroposelective synthesis of axially chiral aryltriazoles.

J. Am. Chem. Soc. *144*, 6200–6207. https://doi.org/10.1021/jacs.2c02563.

69. Guo, W.-T., Zhu, B.-H., Chen, Y., Yang, J., Qian, P.-C., Deng, C., Ye, L.-W., and Li, L. (2022). Enantioselective Rh-catalyzed azide-internal-alkyne cycloaddition for the construction of axially chiral 1,2,3-triazoles. J. Am. Chem. Soc. *144*, 6981–6991. https://doi.org/10.1021/jacs.2c01985.
70. Zeng, L., Li, J., and Cui, S. (2022). Rhodium-catalyzed atroposelective click cycloaddition of azides and alkynes. Angew. Chem. Int. Ed. *61*, e202205037. https://doi.org/10.1002/anie.202205037.
71. Zhou, L., Li, Y., Li, S., Shi, Z., Zhang, X., Tung, C.H., and Xu, Z. (2023). Asymmetric rhodium-catalyzed click cycloaddition to access C-N axially chiral N-triazolyl indoles. Chem. Sci. *14*, 5182–5187. https://doi.org/10.1039/d3sc00610g.
72. Zeng, L., Zhang, F., and Cui, S. (2023). Construction of axial chirality via click chemistry: Rh-catalyzed enantioselective synthesis of 1-triazolyl-2-naphthylamines. Org. Lett. *25*, 443–448. https://doi.org/10.1021/acs.orglett.2c04247.
73. Zeng, L., Li, J., Huang, Y., Haug, G.C., Paton, R.S., Zhang, F., and Cui, S. (2025). Development and mechanistic exploration of rhodium-catalyzed biaxially atroposelective click chemistry. ACS Catal. *15*, 15844–15856. https://doi.org/10.1021/acscatal.5c05278.
74. Qin, C.-Q., Zhao, C., Chen, G.-S., and Liu, Y.-L. (2023). Catalytic enantioselective azide–alkyne cycloaddition chemistry opens up new prospects for chiral triazole syntheses. ACS Catal. *13*, 6301–6311. https://doi.org/10.1021/acscatal.3c00911.
75. Laplante, S.R., Fader, L.D., Fandrick, K.R., Fandrick, D.R., Hucke, O., Kemper, R., Miller, S.P.F., and Edwards, P.J. (2011). Assessing atropisomer axial chirality in drug discovery and development. J. Med. Chem. *54*, 7005–7022. https://doi.org/10.1021/jm200584g.
76. Norberg, S., O'Connor, P.M., Stanton, C., Ross, R.P., Hill, C., Fitzgerald, G.F., and Cotter, P.D. (2011). Altering the composition of caseicins A and B as a means of determining the contribution of specific residues to antimicrobial activity. Appl. Environ. Microbiol. *77*, 2496–2501. https://doi.org/10.1128/AEM.02450-10.
77. Raghothama, S.R., Awasthi, S.K., and Balaram, P. (1998). β-Hairpin nucleation by Pro–Gly β-turns. Comparison of D-Pro–Gly and L-Pro–Gly sequences in an apolar octapeptide. J. Chem. Soc., Perkin Trans. 2 *27*, 137–144. https://doi.org/10.1039/A703331A.
78. Liang, G.B., Rito, C.J., and Gellman, S.H. (1992). Thermodynamic analysis of β-turn formation in Pro-Ala, Pro-Gly, and Pro-Val model peptides in water. J. Am. Chem. Soc. *114*, 4440–4442. https://doi.org/10.1021/ja00037a083.
79. Malde, A.K., Hill, T.A., Iyer, A., and Fairlie, D.P. (2019). Crystal structures of protein-bound cyclic peptides. Chem. Rev. *119*, 9861–9914. https://doi.org/10.1021/acs.chemrev.8b00807.
80. Fitzkee, N.C., Fleming, P.J., Gong, H., Panasik, N., Jr., Street, T.O., and Rose, G.D. (2005). Are proteins made from a limited parts list? Trends Biochem. Sci. *30*, 73–80. https://doi.org/10.1016/j.tibs.2004.12.005.